Available online at www.sciencedirect.com

ScienceDirect

Chinese Journal of Aeronautics 21(2008) 115-124

Chinese Journal of Aeronautics

www.elsevier.com/locate/cja

Active Vibration Control of Beam Using Electro-magnetic Constrained Layer Damping

Niu Hongpan, Zhang Yahong, Zhang Xinong*, Xie Shilin

MOE Key laboratory for Strength and Vibration, Department of Engineering Mechanics, School of Aerospace, Xi'an Jiaotong University, Xi'an 710049, China

Received 31 May 2007; accepted 10 December 2007

Abstract

This paper investigates vibration control of beam through electro-magnetic constrained layer damping (EMCLD) which consists of electromagnet layer, permanent magnet layer and viscoelastic damping layer. When the coil of the electromagnet is electrified with proper control strategy, the electromagnet can exert magnetic force opposite to the direction of structural deformation so that the structural vibration is attenuated. A mathematical model is developed based on the equivalent current method to calculate the electromagnetic control force produced by EMCLD. The governing equations of the system are obtained using Hamilton's Principle and then reduced with the assumed-mode method. A simulation on vibration control of a cantilever beam is conducted under the velocity proportional feedback to demonstrate the energy dissipation capability of EMCLD, and the beam system with the same parameter is experimented. The results of experiment and simulation are compared and the results show that the EMCLD is an effective means for suppressing modal vibration. The results also indicate that the beam system has better control performance for larger control current. The EMCLD method presented in this paper provides an applicable and efficient tool for the vibration control of structures.

Keywords: electro-magnetic constrained layer damping (EMCLD); vibration control; active control

1 Introduction

The constrained layer damping (CLD) treatment has been recognized as an effective way to suppress the vibration of structures. Some researchers have reported their theories and techniques in this field for passive/active vibration control of beams and plates[1-6].

The method of using magnetic material as constrained layer was firstly introduced by Baz and was called magnetic constrained layer damping (MCLD). The finite element model was developed and the passive control of beams and plates with MCLD was studied[7-9]. Then, J.Oh introduced the electro-magnetic damping treatment by which the deformation of viscoelastic damping layer can be actively modulated through electro-magnetic forces[10-11]. Zheng and Zeng conducted a study on the vibrational characteristics of a sandwich cantilever beam partially covered with electro-magnetic damping layer[12-15]. The active and passive magnetic constrained damping treatment was also investigated by the same authors[16].

The modeling of electromagnetic control force is essential for characterizing adequately dynamics of the system with electro-magnetic constrained layer damping (EMCLD). Ref.[10] employed the finite element method to calculate the magnetic and electromagnetic control force, but not gave the relationship between the force and magnetic parameters. In this paper, a mathematical model is

*Corresponding author. Tel.: +86-29-82668757-806.
E-mail address: xnzhang@mail.xjtu.edu.cn
Foundation item: National Natural Science Foundation of China (50275114)

developed based on the equivalent current method to calculate the electromagnetic control force between the electromagnet and the permanent magnet.

In the analysis of viscoelastic damping layer, Ref.[10] resumed that the shear strain of damping layer is not changed along the thickness direction, and thus negatively affected the accuracy of the model. In this paper, both the thickness deformation and the shear strain changing with the thickness are considered.

This paper is organized in seven sections. In Section 1 a brief introduction is given. In Section 2 the concept of EMCLD is introduced and the electromagnetic control force is given. In Section 3 the model of the beam system is built using Hamilton's Principle. The numerical simulation of cantilever beam with EMCLD is conducted in Section 4 and the experimental result is given in Section 5. The comparison of simulational result and experimental result is discussed in Section 6. Section 7 gives the conclusions.

2 Theory of EMCLD

Fig.1 illustrates the configuration of EMCLD in which a viscoelastic damping layer is sandwiched between an electromagnet and a permanent magnet. The permanent magnet is bonded to the controlled beam structure, while the electromagnet is made up of the coil and an aluminum core and acts as cover sheet. When the coil of the electromagnet is electrified, the electromagnet can exert magnetic control force opposite to the direction of structural deformation so that the vibrational energy will be dissipated and thus the structural vibration will be attenuated.

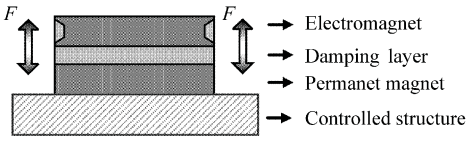

Fig.1 Configuration of EMCDL.

A mathematical model for calculating the magnetic force between the electromagnet and the permanent magnet is developed based on the theory of equivalent current. Fig.2 shows the configuration and geometric properties of the electromagnet and permanent magnet pair. The permanent magnet of thickness h_3 is located below the electromagnet of thickness h_1. The distance between the two magnets is h_2. Both of the magnets have the length a and the width b.

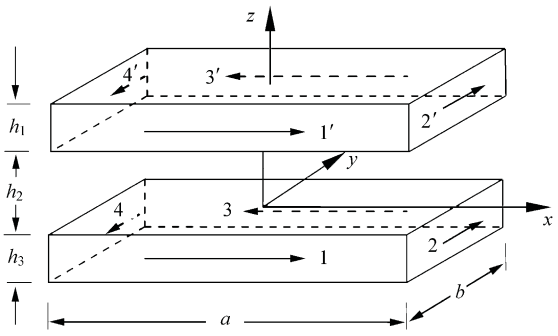

Fig.2 Model of electromagnet and permanent magnet.

It is assumed that the permanent magnet is uniformly magnetized with magnetization M and oriented in the z direction. The relationship between magnetization M and residual induction B_r is $M = B_r/\mu_0$, where μ_0 is the relative permeability of vacuum. According to the assumption of the molecular current, the magnetic moment of the permanent magnet can be represented in terms of the volume current density and the surface current density. The volume current density is given by

$$j_m = \nabla \times M \tag{1}$$

and the surface current density is given by

$$k_m = M \times m \tag{2}$$

where m is the unit vector normal to the surfaces of the magnet.

Because the permanent magnet is uniformly magnetized and oriented in the z direction, the volume current vanishes and the surface current density becomes zero in the top and bottom surfaces of the permanent magnet so that only four surfaces have the equivalent currents. These rectangular surfaces (denoted by 1, 2, 3 and 4) are shown in Fig.2.

Fig.3 gives a schematic diagram for the computation of magnetic force between the surface 1 of

the permanent magnet and the surface 1′ of the electromagnet. From Eq.(2), the equivalent current density of surface 1 is k_{m}, while the surface 1′ has n turns coil with current I.

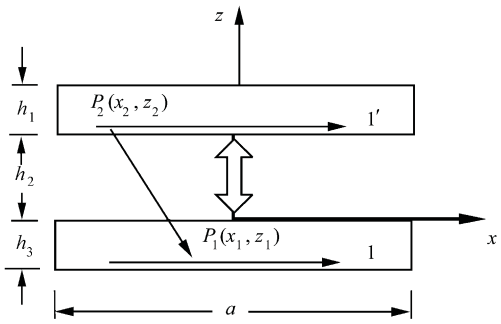

Fig.3 Schematic diagram for the computation of magnet force between the surface 1 of permanent magnet and the surface 1′ of electromagnet magnet.

The value of magnetic induction density at the point $P_1(x_1, z_1)$ produced by point $P_2(x_2, z_2)$ is given by Biot-Savart's law

$$\mathrm{d}\boldsymbol{B}_1 = \frac{\mu_0}{4\pi}\frac{\boldsymbol{I}\mathrm{d}l\times\boldsymbol{r}}{|\boldsymbol{r}|^3} = \frac{\mu_0|\boldsymbol{I}|\boldsymbol{e}_y}{4\pi}\frac{|z_1-z_2|\mathrm{d}x_2}{\left((x_1-x_2)^2+(z_1-z_2)^2\right)^{3/2}} \tag{3}$$

where $\boldsymbol{r}$ is the vector from point P_2 to point P_1 and $\boldsymbol{e}_y$ denotes the unit vector directed to y axis. Thus $\mathrm{d}\boldsymbol{B}_1$ is pointed to the y direction.

The value of magnetic induction $\mathrm{d}\boldsymbol{B}$ at point $P_1(x_1, z_1)$ which is produced by the current on the surface 1′ is

$$\mathrm{d}\boldsymbol{B} = \sum_{i=1}^{n}\int_{-a/2}^{a/2}\mathrm{d}\boldsymbol{B}_1 \tag{4}$$

According to Ampere law, the magnetic force $\mathrm{d}\boldsymbol{F}_{x_1z_1}$ at the point $P_1(x_1, z_1)$ produced by the current on the surface 1′ is given by

$$\mathrm{d}\boldsymbol{F}_{x_1z_1} = k_{\mathrm{m}}\mathrm{d}x_1\mathrm{d}z_1\times\mathrm{d}\boldsymbol{B} \tag{5}$$

The magnetic force of x_1 at permanent magnetic face 1 which is produced by electromagnetic face 1′ is given by

$$\boldsymbol{F}_{1'-1}(x_1) = \int_{-h_3}^{0}\mathrm{d}\boldsymbol{F}_{x_1z_1}(x_1)\mathrm{d}z_1 \tag{6}$$

The magnetic force $\boldsymbol{F}_{1'-1}(x_1)$ is pointed to the z direction.

In the same manner, the magnetic force of x_1 at permanent magnetic face 1 which is produced by electromagnetic face 3′ is

$$\boldsymbol{F}_{3'-1}(x_1) = \int_{-h_3}^{0}\mathrm{d}\boldsymbol{F}_{x_3z_1}(x_1)\mathrm{d}z_1 \tag{7}$$

The current at electromagnetic faces 2′ and 4′ is orthogonal with the current at permanent magnetic face 1, thus the electromagnetic force between these faces is zero. The magnetic force of x_1 at permanent magnetic face 1 which is produced by electromagnet can be get by

$$\boldsymbol{F}_{\mathrm{m1}} = \boldsymbol{F}_{1'-1}(x_1) + \boldsymbol{F}_{3'-1}(x_1) \tag{8}$$

In the same manner, the magnetic forces of faces 2, 3 and 4 which are produced by electromagnet are shown in Fig.4(a). In the direction of x the distributed magnetic force is shown in Fig.4(b) and the electromagnetic force $F_{\mathrm{m}}(x)$ can be given by

$$\boldsymbol{F}_{\mathrm{m}}(x) = \boldsymbol{F}_{\mathrm{m1}}(x) + \boldsymbol{F}_{\mathrm{m3}}(x) \tag{9}$$

in which $\boldsymbol{F}_{\mathrm{m1}}(x)$ and $\boldsymbol{F}_{\mathrm{m3}}(x)$ are distributed magnetic forces of permanent magnetic face 1 and face 3 produced by electromagnet respectively. At the boundaries there are concentrate forces, at left boundary which is $\boldsymbol{F}_{y1} = \int_0^b \boldsymbol{F}_{\mathrm{m4}}(y)\mathrm{d}y$, and at right boundary which is $\boldsymbol{F}_{y2} = \int_0^b \boldsymbol{F}_{\mathrm{m2}}(y)\mathrm{d}y$.

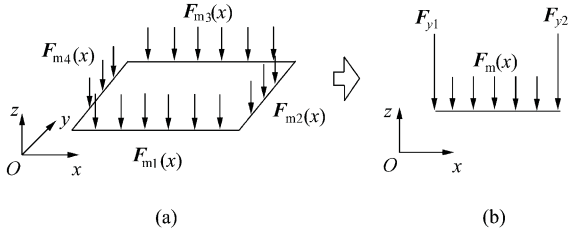

Fig.4 Schematic of magnetic forces in permanent magnet.

From Eqs.(3)-(7), the relationship of magnetic force $\boldsymbol{F}_{\mathrm{m}}(x)$ and the coil current $\boldsymbol{I}$ can be expressed as

$$|\boldsymbol{F}_{\mathrm{m}}(x)| = C_{\mathrm{m}}|\boldsymbol{I}(x)| \tag{10}$$

where C_{m} is the coefficient of EMCLD and at the boundaries, $|\boldsymbol{F}_{y1}| = C_{y1}|\boldsymbol{I}|$ and $|\boldsymbol{F}_{y2}| = C_{y2}|\boldsymbol{I}|$. If the parameters of EMCLD are fixed, the C_{m}, C_{y1} and C_{y2} are constant.

3 Governing Equations

In order to facilitate the derivation of equations of motion, it is assumed that: ① the beam, the electromagnet and the permanent magnet are all purely linear elastic and isotropic, while the damping layer is made of linear viscoelastic material (VEM) with a loss factor of η; ② both the transverse and longitudinal displacements of viscoelastic layer are varying linearly across the thickness; ③ the permanent magnet is bonded perfectly to the beam so that they can be treated as a single layer; ④ there are perfect bonds between all layers with no any slippages; ⑤ all deformations are small and the nonlinear effects are negligible. It should be noted that the transverse displacement of the electromagnet is different from that of the beam due to the effect of compressional deformation of the viscoelastic layer.

A beam with EMCLD is shown in Fig.5. The beam has length of l, width of b and thickness of h_4. The EMCLD has width of b and the boundary coordinates are x_1 and x_2. The thickness of electromagnet, damping layer and permanent magnet are h_1, h_2 and h_3, respectively. It is assumed that the permanent magnet and the beam can be treated as a single layer (PMB) and they have the same neutral face.

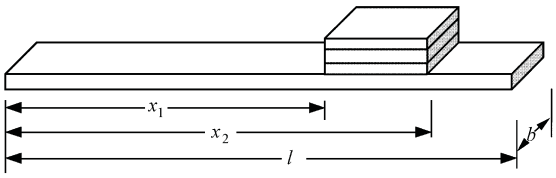

Fig.5 The beam with EMCLD.

The deforming of the beam system is shown in Fig.6. In the z direction, the neutral face deformation of electromagnet is w_1 and that of the PMB is w_3. In the x direction, the neutral face deformation of electromagnet is u_1 and that of the PMB is u_3.

The equations of motion of the beam system can be obtained through the Hamilton's principle, which states

$$\delta\int_{t_1}^{t_2}(T-U+W)\mathrm{d}t=0 \tag{11}$$

where T is the kinetic energy, U the potential energy, W the work done by external force, and δ the variation operator. The beam system is a continuum, thus T, U and W are given through integration over the volume.

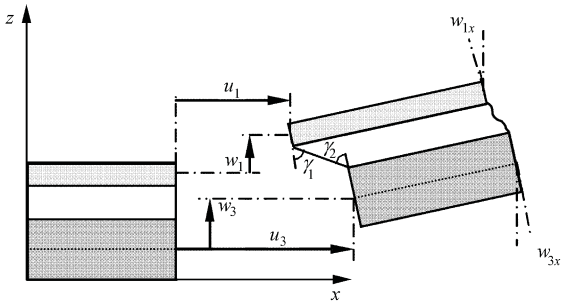

Fig.6 The coordinates of beam with EMCDL.

Here, the Heaviside step function $R(x) = [H(x-x_1) - H(x-x_2)]$ is introduced to express the position of EMCLD for convenience, where H denotes the Heaviside step function, and x_1 and x_2 are the boundary coordinates of EMCLD.

Using $R(x)$, the kinetic energy of beam system can be written as

$$\begin{aligned}T=\frac{1}{2}\int_0^l R(x)\Bigg\{&\left(\rho_1A_1+\frac{\rho_2A_2}{2}\right)\left[\left(\frac{\partial w_1}{\partial t}\right)^2+\left(\frac{\partial u_1}{\partial t}\right)^2\right]+\\&\left(\rho_3A_3+\frac{\rho_2A_2}{2}\right)\left[\left(\frac{\partial w_3}{\partial t}\right)^2+\left(\frac{\partial u_3}{\partial t}\right)^2\right]+\\&\rho_4A_4\left[\left(\frac{\partial w_3}{\partial t}\right)^2+\left(\frac{\partial u_3}{\partial t}\right)^2\right]\Bigg\}\mathrm{d}x\end{aligned} \tag{12}$$

where ρ_i (i = 1, 2, 3, 4) is the density of ith layer and $A_i = bh_i$ is the area of ith layer.

The strain energy of electromagnet layer, permanent magnet and beam is given by

$$\begin{aligned}U=\frac{1}{2}\int_0^l R(x)\Bigg[&E_1I_1\left(\frac{\partial^2 w_1}{\partial x^2}\right)^2+E_1A_1\left(\frac{\partial u_1}{\partial x}\right)^2+\\&E_3I_3\left(\frac{\partial^2 w_3}{\partial x^2}\right)^2+E_3A_3\left(\frac{\partial u_3}{\partial x}\right)^2+\\&E_4I_4\left(\frac{\partial^2 w_3}{\partial x^2}\right)^2+E_4A_4\left(\frac{\partial u_3}{\partial x}\right)^2\Bigg]\mathrm{d}x\end{aligned} \tag{13}$$

where E_i denotes the elastic modulus of ith layer, $I_i = bh_i^3/12$ is the moment of inertia of ith layer.

The strain energy of damping layer can be divided into two parts, one is the shear strain energy and the other is induced by the deforming of thickness[17]. The thickness deformation energy is given by

$$V_{2e}=\frac{1}{2}\int_0^l R(x)E_2\frac{1-\nu_2}{1-\nu_2-2\nu_2^2}A_2\left(\frac{w_1-w_3}{h_2}\right)^2\mathrm{d}x \quad (14)$$

where E_2 is the complex elastic modulus of viscoelastic material and has the form of $E_2=E(1+\eta\mathrm{i})$, in which E is the real part of elastic modulus, and i the imaginary unit.

It is assumed that the shear deformation of damping layer has linear relation with thickness. The shear strain of top area is γ_1, and the shear strain of bottom area is γ_2. The shear strain of damping layer can be written by

$$\gamma(\xi)=\gamma_1+\frac{\gamma_2-\gamma_1}{h_2}\xi \quad (15)$$

where ξ is the distance to the top of damping layer.

From Fig.6, the relation of γ_1, γ_2 and the deformation u_1, u_3, w_1 and w_3 can be written as

$$\gamma_1=\left(1+\frac{h_1}{2h_2}\right)\frac{\partial w_1}{\partial x}+\frac{h_5}{2h_2}\frac{\partial w_3}{\partial x}+\frac{u_1-u_3}{h_2} \quad (16)$$

$$\gamma_2=\left(1+\frac{h_5}{2h_2}\right)\frac{\partial w_3}{\partial x}+\frac{h_1}{2h_2}\frac{\partial w_1}{\partial x}+\frac{u_1-u_3}{h_2} \quad (17)$$

in which $h_5=h_3+h_4$ is the total thickness of beam and permanent magnet layer.

From Eq.(15) to Eq.(17), the shear energy of damping layer can be written as

$$V_{2s}=\frac{1}{2}\int_0^l R(x)G_2b\left[\int_0^{h_2}\left(\gamma_1+\frac{\xi(\gamma_2-\gamma_1)}{h_2}\right)^2\mathrm{d}\xi\right]\mathrm{d}x=$$
$$\frac{1}{2}\int_0^l R(x)G_2bh_2\frac{1}{3}\left(\gamma_1^2+\gamma_1\gamma_2+\gamma_2^2\right)\mathrm{d}x \quad (18)$$

where G_2 is the complex shear modulus of VEM.

The work done by external force is

$$W_e=\int_0^l f(x)w_3\mathrm{d}x \quad (19)$$

where $f(x)$ is the distributed external force applied on the beam.

From Eq.(10), the work done by magnetic force is given by

$$W_m=\int_0^l\left[\delta(x_1)F_{y1}+\delta(x_2)F_{y2}+R(x)F_m(x)\right]\cdot$$
$$(w_1-w_3)\mathrm{d}x=\int_0^l\left[\delta(x_1)C_{y1}I+\delta(x_2)C_{y2}I+\right.$$
$$\left.R(x)C_m(x)I\right](w_1-w_3)\mathrm{d}x \quad (20)$$

where $F_m(x)$ denotes the distributed magnetic force, F_{y1} and F_{y2} are the concentrate force applied on the boundary of EMCLD, $\delta(x)$ is Dirac function, and I is the current of coil.

Substituting Eqs.(12)-(20) into Eq.(11) and integrating by parts, the governing equations of the beam system can be achieved

$$(m_1+m_2/2)\ddot{u}_1-E_1A_1u_1''+$$
$$\frac{1}{3}G_2bh_2\left[\frac{3}{h_2^2}(u_1-u_3)+a_5w_1'+a_7w_3'\right]=0 \quad (21)$$

$$R(x)(m_3+m_2/2)+m_4\ddot{u}_3-R(x)E_3A_3u_3''-E_4A_4u_3''+$$
$$R(x)\cdot\frac{1}{3}G_2bh_2\left[\frac{3}{h_2^2}(u_3-u_1)+a_4w_1'+a_6w_3'\right]=0 \quad (22)$$

$$(m_1+m_1/2)\ddot{w}_1+E_1I_1w_1^{\mathrm{IV}}+E_2A_2a_8\frac{1}{h_2^2}(w_1-w_3)+$$
$$\frac{1}{3}G_2bh_2\left(-a_1w_1''-a_3w_3''-a_4u_3''-a_5u_1''\right)=$$
$$C_m(x)I+\delta(x_1)C_{y1}I+\delta(x_2)C_{y2}I \quad (23)$$

$$R(x)(m_3+m_2/2)\ddot{w}_3+m_4\ddot{w}_3+R(x)E_3I_3w_3^{\mathrm{IV}}+$$
$$R(x)\cdot\frac{1}{3}G_2bh_2\left(-a_2w_3''-a_3w_1''-a_6u_3'-a_7u_1'\right)+$$
$$R(x)E_2A_2a_8\frac{1}{h_2^2}(w_3-w_1)+E_4I_4w_3^{\mathrm{IV}}=$$
$$f(x)-R(x)C_m(x)I-\delta(x_1)C_{y1}I-\delta(x_2)C_{y2}I \quad (24)$$

where superscripts denote the partial differential with respect to x and dot (.) denotes partial differential with respect to time.

In which $m_i=\rho_iA_i\quad(i=1,2,3,4)$

$$a_1=1+\frac{3}{2}\frac{h_1}{h_2}+\frac{3}{4}\frac{h_1^2}{h_2^2},\quad a_2=1+\frac{3}{2}\frac{h_5}{h_2}+\frac{3}{4}\frac{h_5^2}{h_2^2}$$

$$a_3=\frac{1}{2}+\frac{3}{4}\frac{h_1}{h_2}+\frac{3}{4}\frac{h_5}{h_2}+\frac{3}{4}\frac{h_1h_5}{h_2^2},\quad a_4=-\frac{3}{2}\frac{1}{h_2}\left(1+\frac{h_1}{h_2}\right)$$

$$a_5=\frac{3}{2}\frac{1}{h_2}\left(1+\frac{h_1}{h_2}\right),\quad a_6=-\frac{3}{2}\frac{1}{h_2}\left(1+\frac{h_5}{h_2}\right)$$

$$a_7=\frac{3}{2}\frac{1}{h_2}\left(1+\frac{h_5}{h_2}\right),\quad a_8=\frac{1-\nu_2}{1-\nu_2-2\nu_2^2}$$

4 Numerical Simulation

4.1 Model reduction

It can be seen that the dynamics of beam system is described by a group of partial differential equations which are inconvenient to be used in system analysis and control design. Here, the assumed-mode method is employed to simplify the governing equations of the system. For this purpose, the modal shape functions of beam are chosen as the bases of series expansion

$$u_1(x,t)=\sum_{j=1}^{N}U_{1j}(x)\alpha_j(t) \tag{25}$$

$$u_3(x,t)=\sum_{j=1}^{N}U_{3j}(x)\beta_j(t) \tag{26}$$

$$w_1(x,t)=\sum_{j=1}^{N}W_{1j}(x)\zeta_j(t) \tag{27}$$

$$w_3(x,t)=\sum_{j=1}^{N}W_{3j}(x)\lambda_j(t) \tag{28}$$

where α_j, β_j, ζ_j and λ_j are the generalized coordinates, and U_{1j}, U_{3j}, W_{1j} and W_{3j} are the assumed modal shape functions of beam.

Substituting Eqs.(25)-(28) into Eqs.(21)-(24), the following ordinary differential equations can be derived

$$\boldsymbol{M}\ddot{\boldsymbol{\eta}}+\boldsymbol{K}^{*}\boldsymbol{\eta}=\boldsymbol{Q}_{\mathrm{g}}+\boldsymbol{U}_{\mathrm{g}} \tag{29}$$

where $\boldsymbol{\eta}=[\alpha_j\ \beta_j\ \zeta_j\ \lambda_j]^{\mathrm{T}}$ is the generalized coordinates, $\boldsymbol{M}$ the mass matrix, $\boldsymbol{K}^{*}$ the stiffness matrix, $\boldsymbol{Q}_{\mathrm{g}}$ the load vector, and $\boldsymbol{U}_{\mathrm{g}}$ the control input vector.

4.2 Control law

From Section 2, it is known that when the coil is electrified, the EMCLD produces active control functions. In order to control the former two modes of the system, the velocity feedback strategy is taken into consideration. This strategy sets the fed current being proportional to the velocity $V_{\mathrm{p}}(x_{\mathrm{p}}, t)$ at the feedback point $P(x_{\mathrm{p}})$ on the beam. It therefore follows that the electromagnet control force of EMCLD is

$$F_{\mathrm{m}}=P_{\mathrm{v}}C_{\mathrm{m}}V_{\mathrm{p}}(x_{\mathrm{p}},\ t) \tag{30}$$

where P_{v} is the adjustable control gain.

4.3 Simulation

The sketch of control system is shown in Fig.7. The length of beam is 0.28 m and its width is 0.02 m. The start and end boundary coordinates of EMCLD are $x_1 = 0.255$ m and $x_2 = 0.280$ m respectively. Permanent magnet material Nd-Fc-B with residual induction $B_{\mathrm{r}} = 1.18$ is used. The electromagnet is made up of 300 turns coil which has allowable current of 0.3 A. The geometric and material properties of the system are summarized in Table 1.

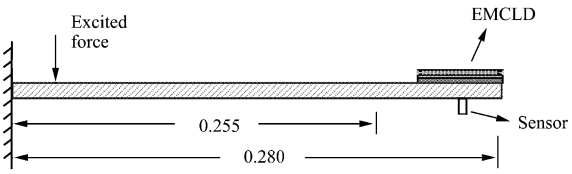

Fig.7 Sketch of the cantilever beam with EMCDL.

Table 1 Geometric and material properties of the system

	Beam	Permanent magnet	VEM	Electro-magnet
E/GPa	71	210	0.001	71
ρ(kg·m^{-3})	2 700	7 300	1 000	2 700
ν	0.3	0.3	0.48	0.3
η	0	0	0.3	0
h/m	0.002	0.001 5	0.001	0.003

4.4 Simulation results

In the simulation, the exciting signal is sine swept signal and applied at $x = 0.008$ m of the beam, and the feedback measurement signal is velocity signal measured at $x = 0.268$ m. The first natural mode is 23.5 Hz and the second is 146.7 Hz. Fig.8 shows the frequency response function (FRF) of beam system, in which the system is not under control, and for active control case the control gain P_{v} = 2, 4, 6. The control performance λs (represented by the reduction percentage of modal response peak) are summarized in Table 2. Compared with not under control case, the active control provides much more significant vibration attenuation for both modes due to the introduction of active action. Fig.8 also shows the FRF under active control with different control gains. It is observed that with the

increase of P_v, the reduction of modal response peak becomes more pronounced. By examining Fig.9, one may conclude that increasing control gain leads to larger driven current and therefore enhances the electromagnetic control force. As a result, the control performance is improved stepwise with the rise of control gain as indicated in Fig.8. Finally, it should be noted that even for the largest control gain P_v = 6, the corresponding control current peak (0.136 A) is still lower than the allowable maximum current of coil (0.3 A).

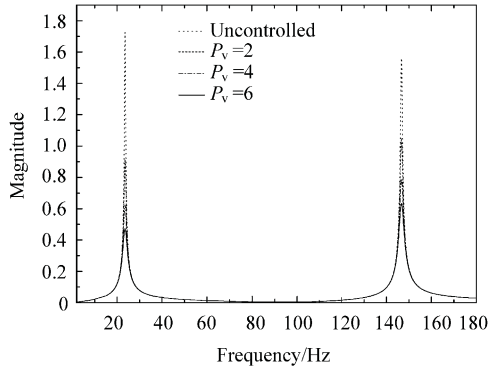

Fig.8 Theoretical control performance of velocity proportional feedback of EMCLD.

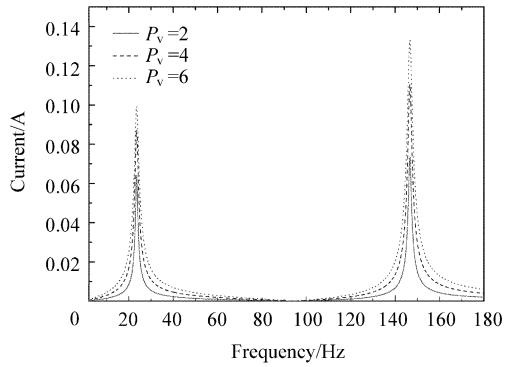

Fig.9 Theoretical control current of velocity proportional feedback of EMCLD.

Table 2 Simulated control performance

	$\lambda(P_v=2)$	$\lambda(P_v=4)$	$\lambda(P_v=6)$
First mode/%	46.9	63.9	72.6
Second mode/%	32.8	49.4	59.4

5 Experimental

5.1 Setup of experiment

The geometrics and material properties of the experiment system, the position of exciting signal and the position of measuring are the same as that of simulation. The sketch of experimental control system is shown as Fig.10. The control strategy is done by dSPACE system. The first natural frequency of cantilever beam system is 17.7 Hz and the second is 150.4 Hz.

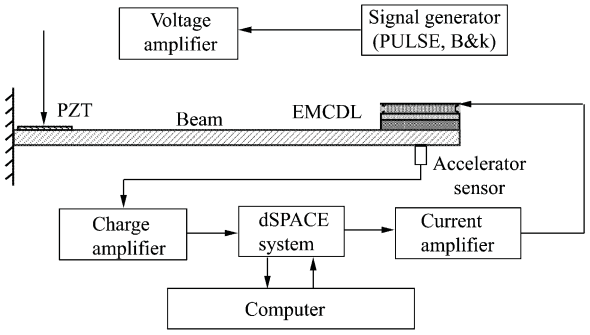

Fig.10 Sketch of the experimental control system of cantilever the beam with EMCDL.

5.2 Vibration control of single mode

The response of the system under velocity feedback control when excited by the first mode signal is shown as Fig.11(a) and the control current is shown in Fig.11(b). The amplitude of response is reduced by 42.3%. The response of second mode is shown as Fig.12(a) and the control current is shown in Fig.12(b). The amplitude of response is reduced by 56.6%. From the curve, at the beginning of control, the current amplitude is bigger and then becomes smaller as the vibration suppression is applied. The stable currents are 0.106 A and 0.105 A, both are under allowable current.

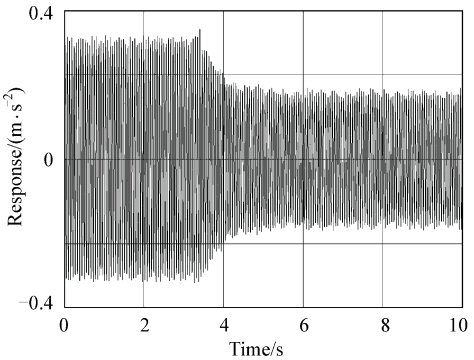

(a)

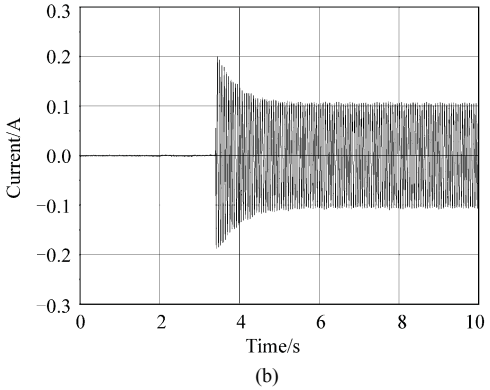

Fig.11 Control performance and control current for the first mode of beam.

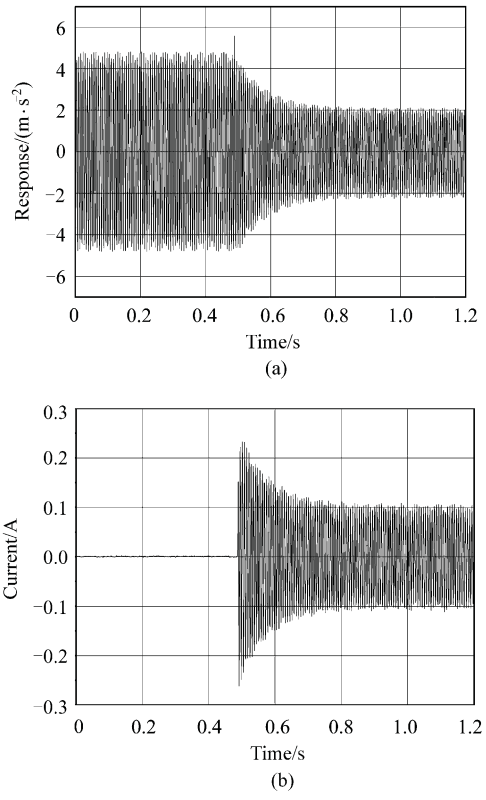

Fig.12 Control performance and control current for the second mode of beam.

5.3 Vibration control of sine swept signal

In the experimental study, for getting the characteristics of beam system, the sine swept signal (0-200 Hz) is applied. Fig.13 shows the FRF of beam system, in which the system is not under control, and for active control case with the control gain $P_v = 2$, 4, 6. For active control case, the control performances are summarized in Table 3. It is observed that with the increase of P_v, the reduction of modal response peak becomes more pronounced. Fig.14 shows the increasing control gain leads to larger driven current, and even for largest gain P_v = 6, the corresponding con trol current peak (0.138 A) is still lower than the allowable current of coil (0.3 A).

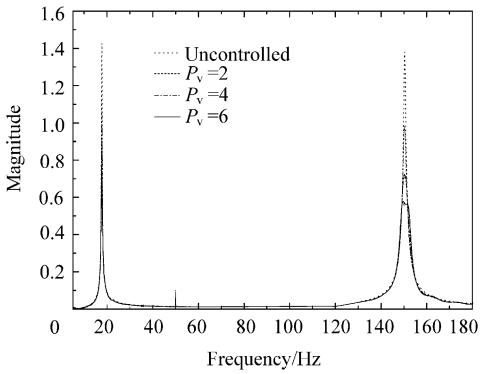

Fig.13 Experimental control performance of velocity proportional feedback of EMCLD.

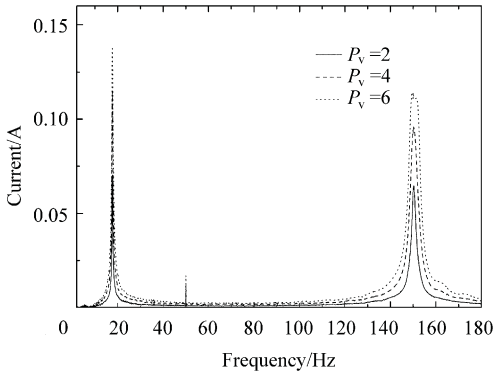

Fig.14 Experimental control current of velocity proportional feedback of EMCLD.

Table 3 Control performance of the experiment

	$\lambda(P_v=2)$	$\lambda(P_v=4)$	$\lambda(P_v=6)$
First mode/%	21.5	37.3	49.2
Second mode/%	25.3	44.2	56.1

6 Comparison Between Experiment and Simulation

Fig.15 shows the comparison between the control performances of experiment and simulation under first mode signal excitation, and that under second mode is shown in Fig.16. From these figures, we can find that the experimental result is worse than simulation result. The main reason is that the delay is existing in experimental study and affects the control performance. The comparison between the control currents of experiment and simulation are shown in Fig.17 and Fig.18. From these figures,

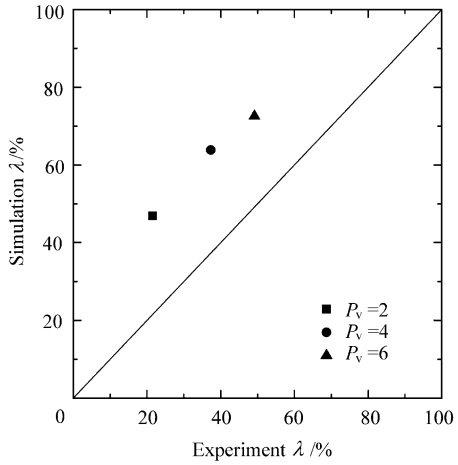

Fig.15 Comparison between the theoretical control performance and the experimental control performance under first mode.

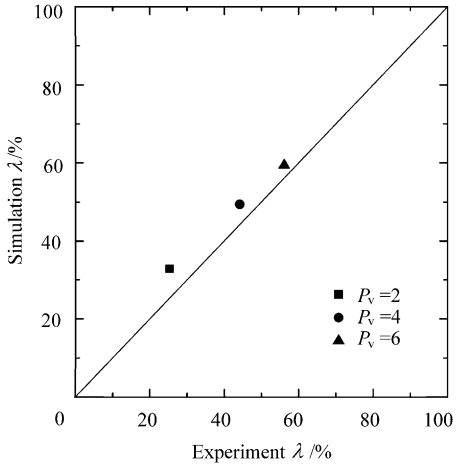

Fig.16 Comparison between the theoretical control performance and the experimental control performance under second mode.

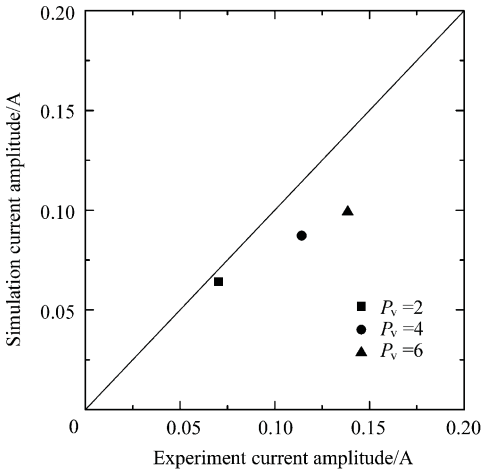

Fig.17 Comparison between the theoretical control current and the experimental control current under first mode.

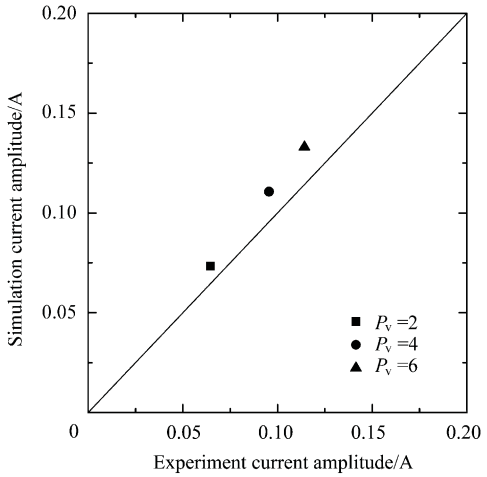

Fig.18 Comparison between the theoretical control current and the experimental control current under second mode.

we can see that the experimental result and simulation result are very close, that verifies the correctness of EMCLD control theory.

7 Conclusions

In this paper the active vibration control of beam structure using EMCLD is investigated. The magnetic control force is calculated based on the assumption of equivalent current. The governing equations of the system are derived using Hamilton principle and then reduced to the discrete series with the assumed-mode method. The application of EMCLD to a cantilever beam is simulated and experimented with velocity feedback control strategy. The simulation results are in agreement with the experimental results.

The frequency response function indicates that active control using EMCLD can suppress modal vibration of beam effectively. Velocity feedback can depress the vibration of both first and second modes. The control performance illustrates that the active control has better control performance as increasing current of coil. The EMCLD method presented in this paper provides an applicable, efficient tool for the vibration control of the structures.

References

[1] Shen I Y. Hybrid damping through intelligent constrained layer damper. ASME Journal of Vibration and Acoustic 1994; 116(3):

341-349.

[2] Zhang X N, Zhang J H. The hybrid control of vibration of thin plate with active constrained damping layer. Applied Mathematics and Mechanics 1998; 19(12): 1035-1048. [in Chinese]

[3] Zhang X N, Li J B, Xie S L, et al. Experimental study on the vibration control of plate with controllable constrained damping layer. Journal of Experimental Mechanics 1999; 14(04): 437-444. [in Chinese]

[4] Du H P, Shi Y M, Zhang L, et al. Research progresses on vibration control of active constrained layer damping. Advances in Mechanics 2001(4): 547-554. [in Chinese]

[5] Liu T X, Shi Y M, Hua H X, et al. A survey on vibration damping and control using active constrained layer damping. Journal of Vibration and Shock 2001(2): 1-6. [in Chinese]

[6] Baz A, Chen T. Control of axi-symmetric vibrations of cylindrical shells using active constrained layer damping. Thin Walled Structures 2000; 36: 1-20.

[7] Ebrahim A K, Baz A. Vibration control of plates using magnetic constrained layer damping. SPIE—The International Society for Optical Engineering 1998; 3327: 138-158.

[8] Oh J, Ruzzene M, Baz A. Control of the dynamic characteristics of passive magnetic composites. Composites Part B: Engineering 1999; 30(7): 739-751.

[9] Ruzzene M, Oh J, Baz A. Finite element modelling of magnetic constrained layer damping. Journal of Sound and Vibration 2000; 236(4): 657-682.

[10] Oh J, Poh S, Ruzzene M, et al. Vibration control of beams using electro-magnetic compressional damping treatment. Journal of Vibration and Acoustics 2000; 122(3): 235-243.

[11] Omer A, Baz A. Vibration control of plates using electromagnetic compressional damping treatment. Journal of Intelligent Material Systems and Structures 2000; 11(10): 791-797.

[12] Zheng H M, He Z, Li Y. Vibration attenuation mechanism of magnetic constrained layer damping treatment. Journal of Vibration and Shock 2003; 22(03): 71-74. [in Chinese]

[13] Zheng H M, He Z, Li Y. Vibration analysis of a magnetic constrained double sandwich-type cantilever beam. Chinese Journal of Applied Mechanics 2004; 21(01): 150-153. [in Chinese]

[14] Li M, Zheng H M, He Z, et al. Vibration analysis of a cantilever plate with partially magnetic constrained damping treatment. Journal of Huazhong University of Science and Technology: Nature Science 2005; 33(10): 25-28. [in Chinese]

[15] Zheng H, Zeng H E. Influence of permanent magnets on vibration characteristics of a partially covered sandwich cantilever beam. Journal of Sound and Vibration 2004; 274(3-5): 801-819.

[16] Zheng H, Li M, He Z. Active and passive magnetic constrained damping treatment. International Journal of Solids and Structures 2003; 40(24): 6767-6779.

[17] Miles R N, Reinhall P G. An analytical model for the vibration of laminated beams including the effects of both shear and thickness deformation in the adhesive layer. Journal of Vibration, Acoustics, Stress, and Reliability in Design 1986; 108(1): 56-64.

Biographies:

Niu Hongpan Born in 1981, he works as a Ph.D. candidate in Xi'an Jiaotong University. His main research interest is passive and active vibration control of structure.
E-mail: skynew@mail.xjtu.edu.cn

Zhang Xinong Born in 1954, he is working for Xi'an Jiaotong University as a professor and doctoral supervisor. His main research interests are vibration control, intelligent strategy, modeling theory, and model analysis.
E-mail: xnzhang@mail.xjtu.edu.cn